



Discovery of inhibitors of the channel-activating protease prostatic (CAP1/PRSS8) utilizing structure-based design

David C. Tully^{a,*}, Agnès Vidal^a, Arnab K. Chatterjee^a, Jennifer A. Williams^a, Michael J. Roberts^a, H. Michael Petrassi^a, Glen Spraggon^a, Badry Bursulaya^a, Reynand Pacoma^a, Aaron Shipway^a, Andrew M. Schumacher^a, Henry Danahay^b, Jennifer L. Harris^a

^a Genomics Institute of the Novartis Research Foundation, 10675 John J. Hopkins Dr., San Diego, CA 92121, USA

^b Novartis Institute for Biomedical Research, Wimblehurst Road, Horsham RH12 5AB, UK

ARTICLE INFO

Article history:

Received 12 June 2008

Revised 8 August 2008

Accepted 11 August 2008

Available online 14 August 2008

Keywords:

Prostasin

PRSS8

hCAP

Channel-activating protease

ENaC activation

Peptidomimetic

Ketoheterocycle inhibitor

ABSTRACT

Structure-based design was utilized to guide the early stage optimization of a substrate-like inhibitor to afford potent peptidomimetic inhibitors of the channel-activating protease prostasin. The first X-ray crystal structures of prostasin with small molecule inhibitors bound to the active site are also reported.

© 2008 Elsevier Ltd. All rights reserved.

Prostasin (CAP1/PRSS8) is a glycosylphosphatidyl-inositol-linked (GPI) serine protease of the chymotrypsin-fold that is expressed in the airway epithelium.^{1,2} Although the physiological substrates of the catalytic activity are not known, prostasin has been shown to be an activator of the epithelial sodium channel (ENaC).^{3,4} Indeed, coexpression of prostasin and ENaC increases the sodium current in *Xenopus* oocytes,^{3,4} whereas siRNA knock-down attenuates the amiloride-sensitive sodium current in a cystic fibrosis airway epithelial cell line.⁵ Recent findings suggest that a proteolytic cascade involving prostasin regulates Na⁺ absorption in the airway, and that abnormal prostasin expression contributes to the excessive proteolytic activation of ENaC in cystic fibrosis patients.⁶ Since ENaC and other ion transport processes control the luminal osmolarity required for normal lung function, it is believed that inhibition of upstream ENaC activators such as prostasin may be attractive therapeutic targets in the treatment of cystic fibrosis.

To date, no small molecule inhibitors of prostasin have been reported. High-throughput screening efforts yielded no viable starting points for medicinal chemistry, so we instead turned to a rational design strategy of peptidomimetic inhibitors using the

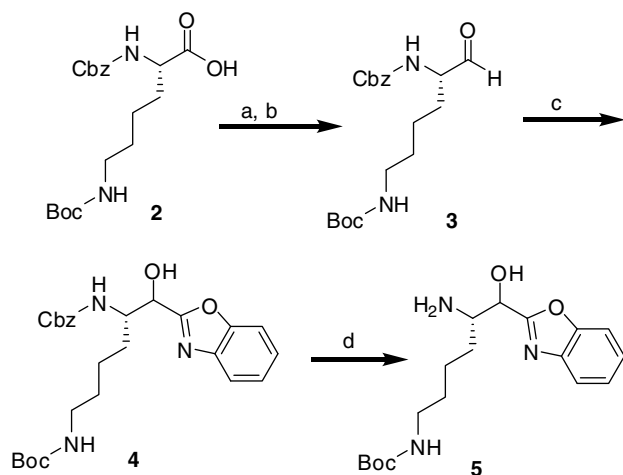
known substrate specificity of prostasin² as a template. By employing positional scanning combinatorial substrate libraries, we have shown previously that prostasin exhibits trypsin-like substrate specificity with a strong preference for arginine or lysine in P1, large hydrophobic amino acids in P2, and basic residues P3.² Here, we report the discovery of potent, reversible inhibitors of prostasin that were initially developed using a substrate mimic approach as a starting point, and then optimized with the aid of the crystal structure of prostasin to improve binding affinity.

We sought to convert our optimized peptide substrate Ac-KHYR-acmc **1** into an inhibitor by replacing the labile coumarin amide with an electrophilic transition-state analog mimic. To accomplish this, we chose α -ketoheterocycle transition-state analogs, which are well-known reversible warheads extensively employed in serine protease inhibitors.^{7–9} The synthesis of the preferred P1-lysine α -ketobenzoxazole intermediate **5** is shown in Scheme 1, starting with commercially available Cbz-Lys(Boc)-OH **2** which was converted to the corresponding aldehyde **3** in two steps. Grignard addition of benzoxazole to the aldehyde **3** gave alcohol **4**, and the subsequent hydrogenolysis of the Cbz protecting group afforded the aminoalcohol **5** as a mixture of diastereomers.

A small number of transition-state analog substrate mimics (compounds **8–13**, Table 1) were initially made using the standard peptide coupling (HATU) and hydrogenolysis conditions shown in

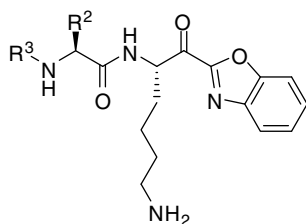
* Corresponding author. Tel.: +1 8588121559; fax: +1 8588121648.

E-mail address: dtully@gnf.org (D.C. Tully).



Scheme 1. Reagents and conditions: (a) *i*-iso-BuOCOCl, Et₃N, THF; ii-NaBH₄, H₂O, 63%; (b) Dess–Martin periodinane, CH₂Cl₂; (c) *iso*-PrMgCl, benzoxazole, THF, –20 °C, 30 min, then aldehyde **3**, –20 °C to rt, 31–48% yield combined steps b and c; (d) H₂ (40 psi), EtOH, Pd/C, rt, 18 h, 69%.

Table 1
Prostasin inhibition constants (*K_i*) for early substrate-like transition-state analogs^a

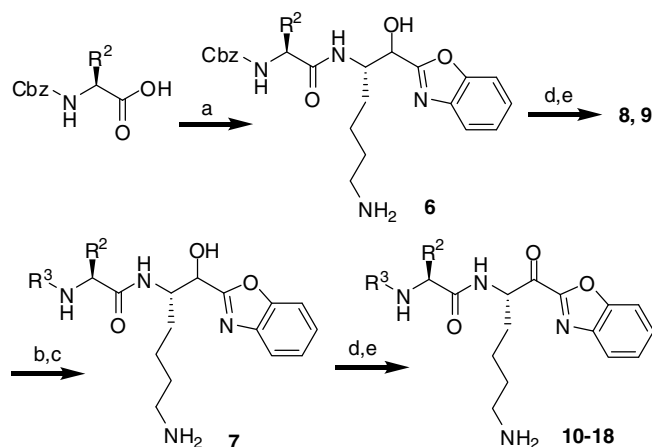


Compound	R ³	R ²	Prostasin <i>K_i</i> (μM)
8	Cbz	–CH ₂ CH(CH ₃) ₂	>100
9	Cbz	–CH ₂ CH ₂ Ph	>100
10	Cbz-Lysine	–CH ₂ CH(CH ₃) ₂	15.2
11	Cbz-Histidine	–CH ₂ CH(CH ₃) ₂	5.72
12	Cbz-Lysine	–CH ₂ CH ₂ Ph	5.78
13	Cbz-Histidine	–CH ₂ CH ₂ Ph	2.10

^a Details of the assay conditions can be found in Ref. 2 and Supplementary material.

Scheme 2, followed by Dess–Martin oxidation of the penultimate alcohol **7**, and deprotection of the Boc groups in the final step. Utilizing the preferred substrate specificity profile of prostasin,² hydrophobic residues leucine and homophenylalanine (hPhe) were initially chosen for P2, while basic residues His and Lys were chosen for P3. Structure–activity relationships in Table 1 clearly demonstrate the requirement for a P3 residue, as truncated analogs **8** and **9** did not inhibit prostasin at concentrations below 100 μM. Introduction of the Cbz-Lys and Cbz-His in P3 (**10–13**) generated several prostasin inhibitors with weak (low μM *K_i*) binding affinity.

The X-ray structure of compound **12** (*K_i* = 5.78 μM) bound to the active site of prostasin is shown in Figure 1, and clearly reveals each of the four subsites (P4–P1) and their respective interactions. The α-ketobenzoxazole warhead establishes the contacts in the oxyanion hole analogous to previously reported X-ray crystal structures of similar α-ketoheterocycles bound to the active sites of related serine proteases.^{7–10} Key hydrogen bonds along the main chain of the inhibitor include the Gln192 sidechain to the P2 carbonyl and an anti-parallel β-sheet-like conformation between the Gly216 and the P3-lysine moiety. The inhibitor's P1-lysine sidechain establishes a water-mediated H-bond with the sidechain of



Scheme 2. Reagents and conditions: (a) **5**, HATU, DIEA, DCM, rt, 86%; (b) H₂ (40 psi), EtOH, Pd/C, rt, 18 h, 92%. (c) R³COOH, HATU, DIEA, DCM, rt, 81–90%; (d) Dess–Martin periodinane, CH₂Cl₂, 45–65%; (e) TFA/ CH₂Cl₂, reverse-phase HPLC, 75–85%.

Asp189 at the bottom of the S1 pocket, while the P3-lysine is mostly solvent exposed with no obvious interactions. The phenethyl P2 moiety is sandwiched between the Glu97 and Trp215 sidechains, while the N-terminal benzyl group is stacked edge on face with the indole ring of Trp215.

Several clues from the X-ray structure of compound **12** suggest possible directions for the optimization of inhibitor design in order to improve binding affinity. First, the P2 NH clearly does not participate in any H-bonding interactions, suggesting that proline could potentially be tolerated in P2 to add a degree of conformational restraint to the peptidic scaffold. Second, the natural L-configuration of the P3-lysine directs the sidechain out toward solvent, and forces the N-terminal benzyl group into the hydrophobic pocket defined primarily by Trp215, Pro172I, His172J, and Gly98. Using this X-ray structure as a guide, modeling suggested that the opposite configuration of the P3 subunit bearing a hydrophobic sidechain could more efficiently fill this hydrophobic pocket, and take advantage of the π-stacking interaction with Trp215.

Incorporation of these changes into the initial inhibitor design led us to compound **14**, which has a proline in P2 and the opposite configuration D-hPhe in P3 (Table 2). Conformational restraint conferred by the proline in P2 led to a slight improvement in potency

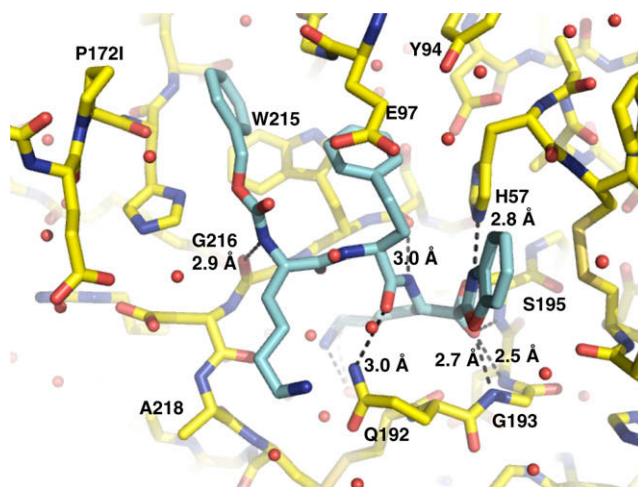
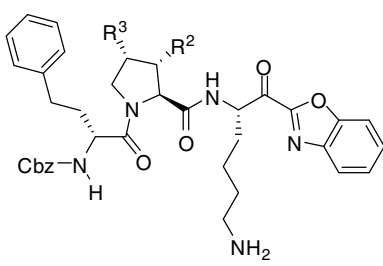


Figure 1. Crystal structure of Prostasin with compound **12** at 1.6 Å resolution (RCSB PDB ID: 3E16). Figure generated using PyMol.

Table 2
Effect of P2 substituents on prostasin inhibition (K_i)



Compound	R ³	R ²	Prostasin K_i (μ M)
14	–H	–H	1.40
15	–H	–Ph	0.267
16	–H	–Me	0.049
17	–OCH ₂ Ph	–H	0.040
18	–OH	–H	1.04
19	–OCH ₂ (<i>meta</i> -CF ₃)Ph	–H	0.041
20	–OCH ₂ (<i>para</i> -CF ₃)Ph	–H	0.028
21	–OCH ₂ (<i>para</i> -Me)Ph	–H	0.045
22	–OCH ₂ (<i>para</i> -F)Ph	–H	0.027
23	–OCH ₂ (<i>para</i> -Cl)Ph	–H	0.012
24	–OCH ₂ -cyclo-C ₆ H ₁₁	–H	0.019
25	–OCH ₂ -cyclo-C ₅ H ₉	–H	0.065
26	–OCONHPh	–H	0.130
27	–OCONHCH ₂ Ph	–H	0.060
28	–OCONHCH ₂ (<i>p</i> -SO ₂ Me)Ph	–H	0.176
29	Piperidinecarbonyloxy–	–H	0.029
30	Pyrrolidinecarbonyloxy–	–H	0.101
31	Morpholinecarbonyloxy–	–H	0.510
32	–OCONMe ₂	–H	1.55

(**14**, K_i = 1.4 μ M) over the previous analogs **10–13**. However, compound **14** lacks a P2 substituent capable of extending into the S2 subsite to pick up any favorable hydrophobic interactions. To achieve this, compound **15** was prepared using the conformationally constrained analog of hPhe in P2 from commercially available (2*R*,3*S*)-3-phenyl-L-proline. Incorporation of a phenyl substituent onto the proline ring resulted in a fivefold improvement in potency (K_i = 0.267 μ M) over **14**, demonstrating the importance of the favorable interaction gained by hydrophobic substituents that are

able to extend into the S2 subsite. Interestingly, the replacement of the phenyl group for a simple methyl group at the proline 3-position (**16**) further improved the potency (K_i = 0.049 μ M). To gain additional insight into the SAR at the P2 position, we next chose to explore the effect of introducing substituents at the synthetically more accessible 4-position of proline. Benzyl ether **17** (K_i = 0.040 μ M) demonstrated that comparable improvements in inhibitory activity could be achieved by the incorporation of hydrophobic substituents at the proline 4-position, while the 4-hydroxy analog **18** (K_i = 1.04 μ M) confirmed that larger hydrophobic substituents were preferred over small polar moieties.

To explore the effect of substituents on the P2 benzyl ring have on the SAR, a small subset of substituted benzyl ethers (**19–25**) were synthesized according to the procedure outlined in Scheme 3 from the commercially available starting material Boc-L-hydroxyproline. Compound **19** (K_i = 0.041 μ M) demonstrated that substitution on the *meta*-position of the benzyl ring has no noticeable effect on potency, while small hydrophobic substituents at the

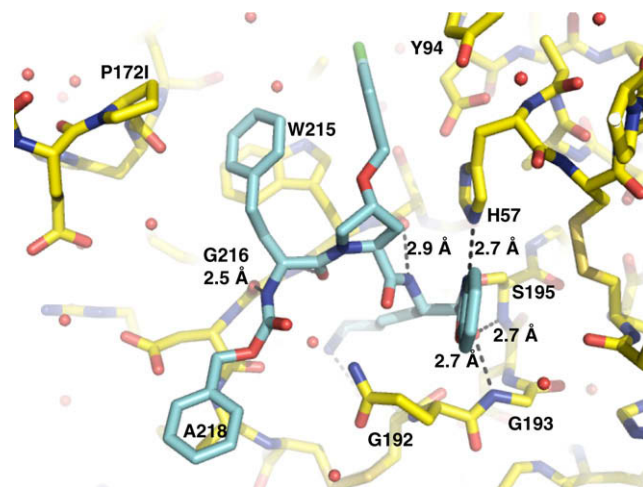
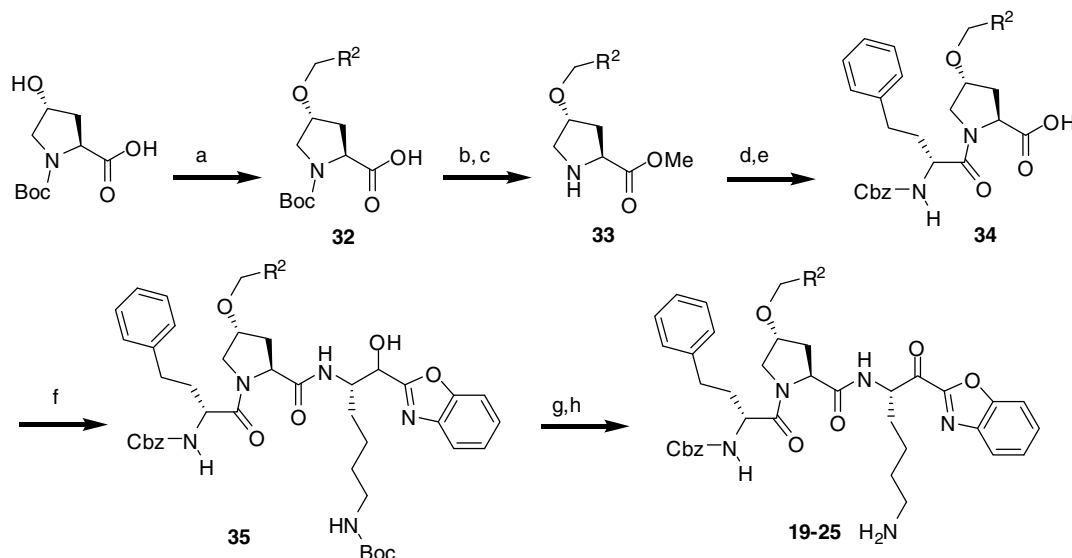
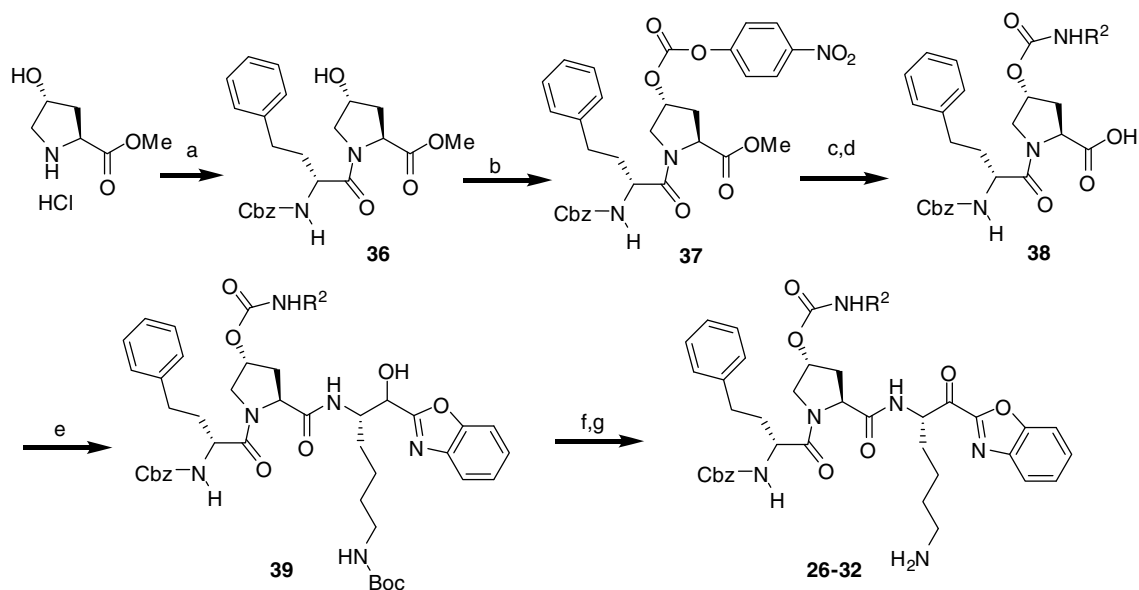


Figure 2. Crystal structure of Prostasin with compound **23** at 1.7 Å resolution (RCSB PDB ID: 3EOP). Figure generated using PyMol.



Scheme 3. Reagents and conditions: (a) i-KOH (8.0 equiv), DMSO, 0 °C, 20 min; ii-R²CH₂Br (4.5 equiv), 0 °C, 15 min, then 20 °C, 4 h, 82%; (b) TMS-CHN₂ (2.0 M in Et₂O), 20% MeOH in CH₂Cl₂, 89%; (c) TFA (50%) in CH₂Cl₂, 100%; (d) Cbz-D-homoPhe-OH, HATU, DIEA, CH₂Cl₂, rt, 84%; (e) LiOH-H₂O, 1,4-dioxane/water 50:50, 85%; (f) **5**, HATU, DIEA, CH₂Cl₂, 73–86%; (g) Dess–Martin periodinane, CH₂Cl₂, 45–65%; (h) TFA/CH₂Cl₂, reverse-phase HPLC, 75–85%.



Scheme 4. Reagents and conditions: (a) Cbz-D-hPhe-OH, HATU, DIEA, CH₂Cl₂, rt, 84%; (b) *para*-nitrophenylchloroformate, pyridine, CH₂Cl₂, 76%; (c) H₂NR², CH₂Cl₂, 72–80%; (d) LiOH·H₂O, 1,4-dioxane/water 50:50, 85%; (e) **5**, HATU, DIEA, CH₂Cl₂, 73–86%; (f) Dess–Martin periodinane, CH₂Cl₂, 45–65%; (g) TFA/CH₂Cl₂, reverse-phase HPLC, 75–85%.

para-position led to modest improvements, with 4-chlorobenzyl ether **23** contributing to a threefold boost in potency ($K_i = 0.012 \mu\text{M}$) compared to **17**. Cycloaliphatic ethers **24** and **25** demonstrate that a cyclohexyl ring (**24**, $K_i = 0.019 \mu\text{M}$) is preferred slightly over cyclopentyl (**25**, $K_i = 0.041 \mu\text{M}$), suggesting that the larger cyclohexyl ring is able to more efficiently occupy the S2 subsite.

A second X-ray crystal structure of prostaticin with compound **23** bound to the active site is shown in Figure 2. The various interactions between the P1-lysine-ketobenzoxazole moiety and the residues of the catalytic triad, oxyanion hole, and S1 subsite are essentially identical to the structure with compound **12**. The noticeable difference arises in the S2 subsite, as the loop containing Glu97, which defines a narrow cleft occupied by the phenethyl group in the structure of compound **12** (Fig. 1), has undergone a significant conformational change in this second structure (Fig. 2). This change accommodates the binding of the *para*-chlorobenzylether moiety into a broad hydrophobic compartment defined primarily by Trp215, Met180, and Tyr94. The adjacent S3 subsite, defined principally by Trp215 and Pro172I, accommodates the P3 phenethyl group. This moiety occupies essentially the same space as the benzylcarbamate moiety of compound **12**, while the N-terminal benzyl group of **23** is now situated over the small hydrophobic patch defined by Ala218.

Next, we explored the SAR around a number of carbamates substituted on the 4-position of the P2 proline subunit (compounds **26–32**), which were synthesized according to the procedure outlined in Scheme 4. Both phenyl and benzyl carbamates **26** and **27** both exhibit a loss of potency from benzyl ether **23**, while addition of a polar sulfone (**28**, $K_i = 0.176 \mu\text{M}$) has a further deleterious effect confirming the S2 subsite's strong preference for non-polar, hydrophobic moieties. Interestingly, the piperidine carbamate **29** ($K_i = 0.029 \mu\text{M}$) is roughly equipotent with cyclohexylmethyl ether **24**, while the pyrrolidine carbamate results in a several-fold loss in inhibitory activity, suggesting again that the six-membered aliphatic rings are able to fill the hydrophobic S2 subsite more efficiently. Morpholine carbamate **31** ($K_i = 0.510 \mu\text{M}$), which drops off more than 17-fold in inhibitory activity from the piperidine analog **29**, again confirms that even a single heteroatom is not well tolerated by the S2 binding pocket. Meanwhile, the dim-

ethylcarbamate **32** ($K_i = 1.55 \mu\text{M}$), which is roughly equipotent to the unfunctionalized proline **14**, demonstrates that small hydrophobic substituents at the proline 4-position make no significant contribution to the binding affinity, in stark contrast to the gain in potency conferred by a methyl substituent at the 3-position of proline (**16**, $K_i = 0.049 \mu\text{M}$). This suggests that a possible binding mode for **16** may be similar to that seen for compound **12**, in which the 90's loop is closed, allowing for this methyl group to derive a hydrophobic interaction within the narrow hydrophobic cleft.

In summary, we have utilized the substrate specificity profile as a template for the first small molecule inhibitors of the channel-activating protease prostaticin. Direct translation of the substrate sequence to an inhibitor sequence resulted only in marginally active compounds. Subsequently, guided by the X-ray structure, we were able to optimize the peptidomimetic scaffold to generate the first low nanomolar K_i inhibitors of prostaticin. The structure–activity relationships surrounding analogs from this scaffold display a clear preference for large, flexible hydrophobic substituents at the 4-position of the P2 proline subunit, whereas at the 3-position of proline, there is a preference for smaller hydrophobic substituents. Structure-based design and medicinal chemistry optimization eventually led to compound **23**, which is a potent, reversible inhibitor of prostaticin with $K_i = 0.012 \mu\text{M}$.

Supplementary data

Supplementary data associated with this article can be found, in the online version, at doi:10.1016/j.bmcl.2008.08.029.

References and notes

- Yu, J. X.; Chao, L.; Chao, J. *J. Biol. Chem.* **1994**, *269*, 18843.
- Shipway, A.; Danahay, H.; Williams, J. A.; Tully, D. C.; Backes, B. J.; Harris, J. L. *Biochem. Biophys. Res. Commun.* **2004**, *324*, 953.
- Adachi, M.; Kitamura, K.; Miyoshi, T.; Narikyo, T.; Iwashita, K.; Shiraishi, N.; Nonoguchi, H.; Tomita, K. *J. Am. Soc. Nephrol.* **2001**, *12*, 1114.
- Donaldson, S. H.; Hirsh, A.; Li, D. C.; Holloway, G.; Chao, J.; Boucher, R. C.; Gabriel, S. E. *J. Biol. Chem.* **2002**, *277*, 8338.
- Tong, Z.; Illek, B.; Bhagwandin, V. J.; Verghese, G. M.; Caughey, G. H. *Am. J. Physiol. Lung. Cell. Mol. Physiol.* **2004**, *287*, L928.
- McKenna, E. E.; Luke, C. J.; Frizzell, R. A.; Kleyman, T. R.; Pilewski, J. M. *Am. J. Physiol. Lung. Cell. Mol. Physiol.* **2008**, *294*, L932.

7. (a) Edwards, P. D.; Meyer, E. F., Jr.; Vijayalakshmi, J.; Tuthill, P. A.; Andisik, D. A.; Gomes, B.; Strimpler, A. *J. Am. Chem. Soc.* **1992**, *114*, 1854; (b) Edwards, P. D.; Wolanin, D. J.; Andisik, D. W.; Davis, M. W. *J. Med. Chem.* **1995**, *38*, 76; (c) Edwards, P. D.; Zottola, M. A.; Davis, M. W.; Williams, J.; Tuthill, P. A. *J. Med. Chem.* **1995**, *38*, 3972.
8. (a) Costanzo, M. J.; Maryanoff, B. E.; Hecker, L. R.; Schott, M. R.; Yabut, S. C.; Zhang, H.-C.; Andrade-Gordon, P.; Kauffman, J. A.; Lewis, J. M.; Krishnan, R.; Tulinsky, A. *J. Med. Chem.* **1996**, *39*, 3039; (b) Costanzo, M. J.; Almond, H. R., Jr.; Hecker, L. R.; Schott, M. R.; Yabut, S. C.; Zhang, H.-C.; Andrade-Gordon, P.; Corcoran, T. W.; Giardino, E. C.; Kauffman, J. A.; Lewis, J. M.; deGaravilla, L.; Haertlein, B. J.; Maryanoff, B. E. *J. Med. Chem.* **2005**, *48*, 1984.
9. A comprehensive review on the subject of α -ketoheterocycle protease inhibitors: Maryanoff, B. E.; Costanzo, M. J. *Bioorg. Med. Chem.* **2008**, *16*, 1562.
10. (a) Matthews, J. H.; Krishnan, R.; Costanzo, M. J.; Maryanoff, B. E.; Tulinsky, A. *Biophys. J.* **1996**, *71*, 2830; (b) Recacha, R.; Costanzo, M. J.; Maryanoff, B. E.; Carson, M.; DeLucas, L. J.; Chattopadhyay, D. *Acta Crystallogr., Sect. D: Biol. Crystallogr.* **2000**, *56*, 1395.